J Mater Sci: Mater Electron (2017) 28:16120–16132
DOI 10.1007/s10854-017-7512-3

Effect of indium addition on interfacial IMC growth and bending properties of eutectic Sn–0.7Cu solder joints

Shuang Tian[1] · Saipeng Li[1] · Jian Zhou[1,2] · Feng Xue[1,2] · Ruihua Cao[1] · Fengjiang Wang[3]

Received: 4 May 2017 / Accepted: 10 July 2017 / Published online: 31 July 2017

Abstract The microstructure and growth behaviors of interfacial IMCs between the Sn–0.7Cu–xIn (x = 0–5.0 wt%) solder and Cu substrate under solid aging were investigated. Bending test was conducted to evaluate the mechanical properties of Cu/Sn–0.7Cu–xIn/Cu solder joints. The needle-like $Cu_6(Sn,In)_5$ IMCs formed at interface instead of Cu_6Sn_5 in as-soldered In-containing solder joints. During solid aging, indium addition had little influence on the growth of Cu_6Sn_5 IMCs, but strongly suppressed the growth of Cu_3Sn IMCs. In Sn–0.7Cu–5.0In/Cu couple, the maximum solubility of indium in Cu_6Sn_5 and Cu_3Sn was about 4.9 and 3.1 at.% respectively which was independent of aging temperature. The average composition of $Cu_6(Sn,In)_5$ and $Cu_3(Sn,In)$ were given as $Cu_6(Sn_{0.89},In_{0.11})_5$ and $Cu_3(Sn_{0.88},In_{0.12})$. After indium addition, the diffusion coefficients were found to be lower than that of Sn–0.7Cu/Cu couple and the activation energy for the growth of Cu_3Sn increased with the increase of indium content. Doping indium into Sn–0.7Cu solder improved the bending properties of solder joints. Interfacial cracks were suppressed effectively after long time aging with indium addition.

✉ Jian Zhou
jethro@seu.edu.cn

[1] Jiangsu Key Laboratory for Advanced Metallic Materials, Southeast University, Nanjing 211189, China

[2] Jiangsu Key Laboratory of Advanced Structural Materials and Application Technology, Nanjing Institute of Technology, Nanjing 211189, China

[3] Provincial Key Lab of Advanced Welding Technology, Jiangsu University of Science and Technology, Zhenjiang 212003, China

1 Introduction

Solder alloy plays a critical role in connecting the electronic components to a substrate in electronic devices. Traditional Sn–Pb solders owning low melting point, good wettability and mechanical properties has been widely applied in microelectronic industry. However, the toxicity of lead and increasing environmental concern limit the application of Sn–Pb solder alloy, accelerating the development of lead-free solder [1–3]. As present, Sn–0.7Cu eutectic alloy is identified as an attractive candidate solder due to its good wettability, mechanical properties and lower cost compared to other lead-free solder alloys. However, the high melting point and rapid growth of interfacial intermetallic compounds (IMCs) need to be further improved. Microalloying as a convenient and effective method to improve the performance of solder alloys has been widely adopted for the last two decades [4, 5]. Some metallic element such as Ag [6, 7], Bi [8], Ni [9–11], Al [12], Zn [13] and Fe [14] has been added into Sn–Cu binary alloy systems.

Soldering is a critical process in electronic packaging. During soldering, IMCs form at the interface between molten solder and substrate. It has been reported that interfacial IMCs are much harder and more brittle than the solder alloy and the overgrown IMCs deteriorate the mechanical properties of solder joints [15]. Various alloying elements have been added into solder alloys to suppress the growth of interfacial IMCs [16–19]. Wang et al. [20] has investigated the interfacial microstructure of Sn–58Bi/Cu and Sn–58Bi/Cu–Zn joints, the formation of Cu_3Sn IMC was depressed, Kirkendall voids and Bi segregation at interface were avoided with minor Zn added into Cu substrate. Yu et al. [21] has found that Zn and Ge were helpful element to suppress the formation of Cu_3Sn layer. With more Zn addition, Cu_6Sn_5 IMC layer varied to Cu–Zn IMC layer and voids were formed at Cu_6Sn_5/Cu–Zn interface. The addition of nano-TiO_2 into Sn–3.0Ag–0.5Cu solder suppressed the growth of Cu_6Sn_5 layer, but has little influence on the growth of Cu_3Sn layer. The adsorption theory and grain boundary pinning were conducted to explain the suppressed growth rate of interfacial IMCs [22]. Indium is well known as a beneficial element to solder alloy, but the influence of indium addition on the reaction between the Sn–Cu solder and Cu substrate is seldom systematically investigated.

In this paper, the effect of indium addition on microstructure and composition of interfacial IMCs between Sn–0.7Cu–xIn (x = 0–5.0 wt%) and Cu substrate was investigated. The growth coefficients at 150, 170 and 190 °C as well as the activation energy of the interfacial IMCs layer were calculated according to the Arrhenius equation. Bending test was conducted to evaluate the mechanical properties of Cu/Sn–0.7Cu–xIn/Cu solder joints. The transformation of fracture mode considering the effect of indium content and aging time was also discussed.

Table 1 Chemical compositions of Sn–0.7Cu–xIn lead-free solder alloy

Alloy	Composition (wt%)		
	Sn	Cu	In
Sn–0.7Cu	Bal.	0.743	ND
Sn–0.7Cu–1.0In	Bal.	0.712	0.984
Sn–0.7Cu–2.0In	Bal.	0.736	2.012
Sn–0.7Cu–3.0In	Bal.	0.698	2.963
Sn–0.7Cu–4.0In	Bal.	0.725	4.149
Sn–0.7Cu–5.0In	Bal.	0.688	5.033

2 Experimental procedures

Predetermined quantities of Sn, Cu and In were melted at 800 °C in a quartz crucible inside a resistance furnace. The molten alloy was held for 60 min and stirred for each 10 min to avoid the segregation of composition. The liquid solder alloys were casted into a steel mold and air-cooled to 25 °C. The analyzed chemical compositions of each Sn–0.7Cu–xIn alloys by inductive couple plasma (ICP) were given in Table 1.

The spreading specimens were prepared by Cu substrate and Sn–0.7Cu–xIn solder on the heating platform at 250 °C for 60 s. To study the growth of the interfacial reaction layer, a set of specimens were isothermal aged by oil bath at three different temperatures of 150, 170 and 190 °C for varying aging time intervals of 120, 240, 480, 720 and 960 h. After isothermal aging, the average thickness of interfacial IMCs was calculated by measuring the total area of the IMCs and dividing it by the total length of the images. For each aging condition, three specimens were examined to obtain the average thickness value of the reaction layer.

Commercial oxygen-free copper sheet in a dimension of 15 × 15 × 1 mm was used as the based metal. The copper surfaces were grinded on sandpapers, mechanically polished to 1 μm with diamond paste, followed by ultrasonically cleaned in acetone. A film of solder alloy with 200 μm in thickness was supplied for soldering. The schematic diagram of the bending joint is illustrated in Fig. 1a. The soldering process was carried out by means of reflow furnace. Sn–0.7Cu–xIn solder films covered with flux between the copper sheets was heated at 250 °C for 60 s, and air-cooled to ambient temperature. After preparation, the joints were aged by oil bath at 190 °C for 240, 480, 720 and 960 h, respectively. The bending strength of solder joints were

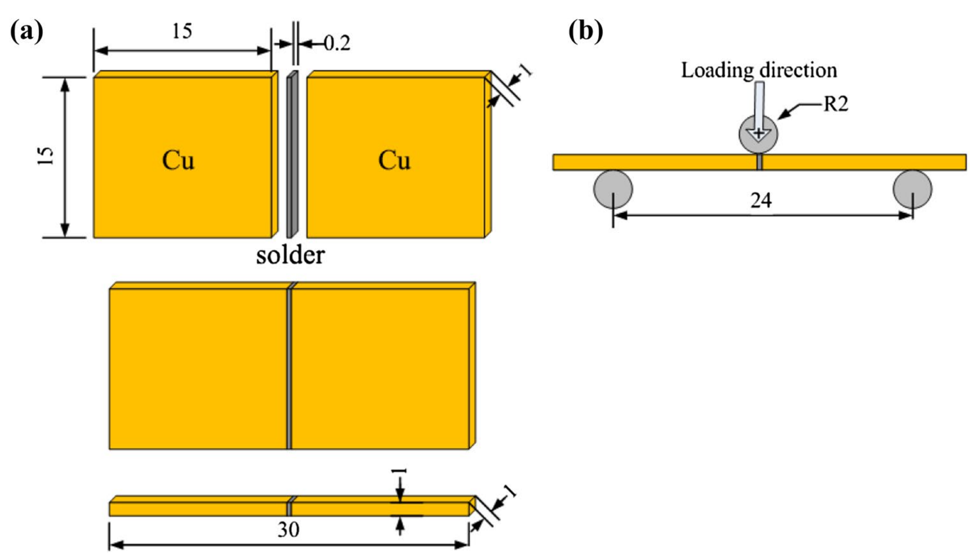

Fig. 1 Schematics on (**a**) bending joints fabrication and (**b**) three point flexural test on bending joints

measured with a three point flexural test method at a loading rate of 0.1 mm/s. The radius of loading point and two supporting points was 2 mm, and the span between the two supporting points was 24 mm as shown in Fig. 1b.

Common metallographic sample preparation method was used for microstructure observation of the cross sections. The specimens were etched with a solution of 5 vol% HNO_3 + 5 vol% HCl + 90 vol% CH_3OH. The microstructure of interfacial IMCs was probed by scanning electron microscopy (SEM). Energy Dispersive X-ray (EDX) was employed to determine the elemental compositions. The accurate compositions of IMCs at interface were identified using X-Ray Diffraction (XRD). During bending test, the initiation and propagation of cracks on the bending joints were also observed by SEM.

3 Results and discussion

3.1 Morphology and compositions of as-soldered IMCs layer

Figure 2 shows the microstructure of interfacial IMCs between Sn–0.7Cu–xIn and Cu substrate after reflow at 250 °C for 60 s. In all cases, a scallop shaped interfacial IMC layer formed at the interface as shown in Fig. 2a, d, g. The scallop shaped interfacial layer was also observed after various solder alloys soldered on Cu substrate, such as Sn–Bi [16, 23], Sn–Ag [24], Sn–Zn [25] and Sn–Ag–Cu [26]. Figure 2b, e, h show the top-view of the interfacial IMCs. The IMCs at Sn–0.7Cu/Cu interface showed a granular morphology and the grain diameter was about 3.1 µm. After 1.0 wt% indium addition, some needle-like IMCs which were much larger than the granular ones were found at the Sn–0.7Cu–1.0In/Cu interface. Similarly, more needle-like IMCs were observed when the indium content was up to 5.0 wt% as shown in Fig. 2h, indicating that indium addition could change the morphology of IMCs at solder/Cu interface.

The composition of the Sn–0.7Cu/Cu interfacial IMCs was Cu–Sn compounds and transformed to Cu–In–Sn compounds with indium addition as shown in Fig. 2c, f, i. To identify the accurate compositions of IMCs, the results of XRD analysis on the top-view of the interfacial IMCs are given in Fig. 3. Cu_6Sn_5 phase was confirmed at the interface of Sn–0.7Cu/Cu. With added indium in Sn–0.7Cu solder, the reaction product with Cu substrate kept the same as Cu_6Sn_5, suggesting the needle-like Cu–In–Sn IMCs found

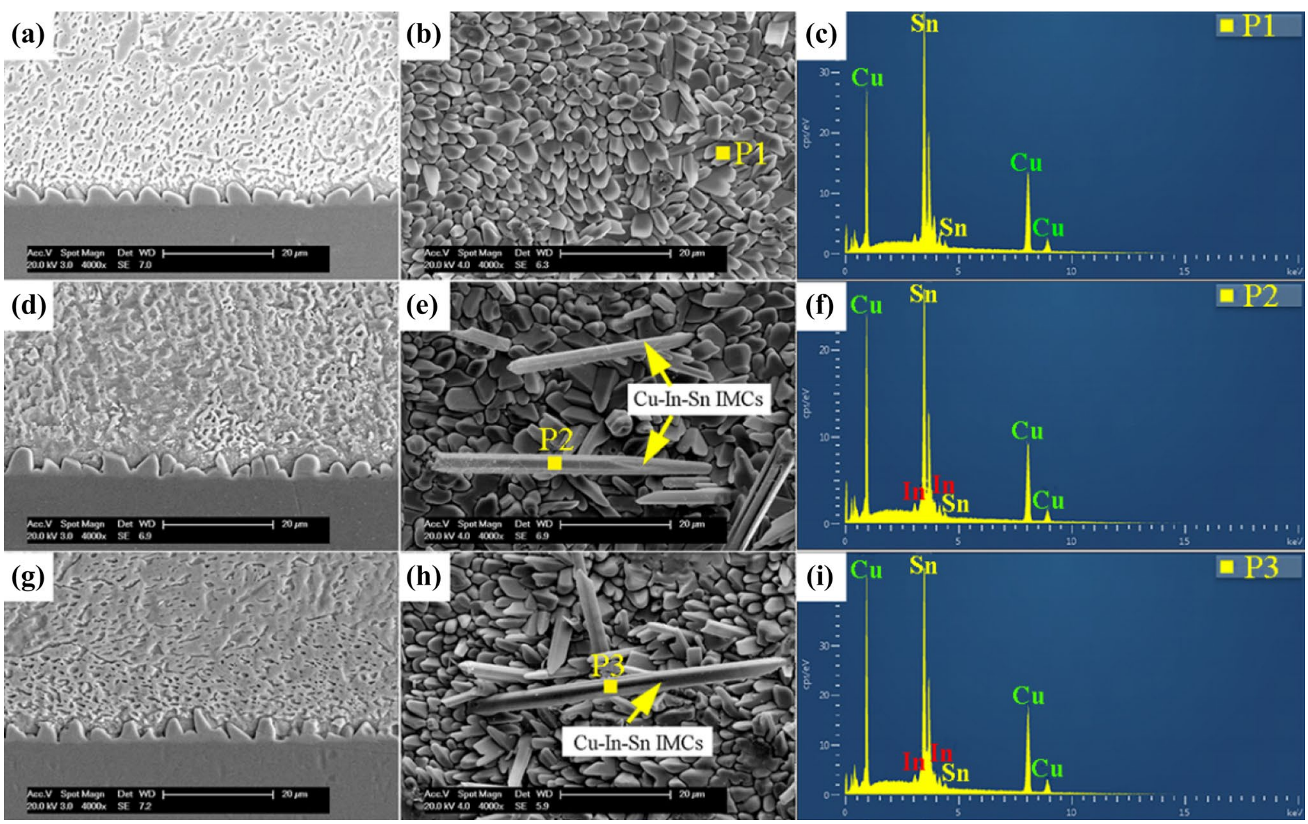

Fig. 2 Microstructure of IMCs layer between Sn–0.7Cu–xIn and Cu substrate reflowed for 1960s: **a–c** Sn–0.7Cu; **d–f** Sn–0.7Cu–1.0In; **g–i** Sn–0.7Cu–5.0In

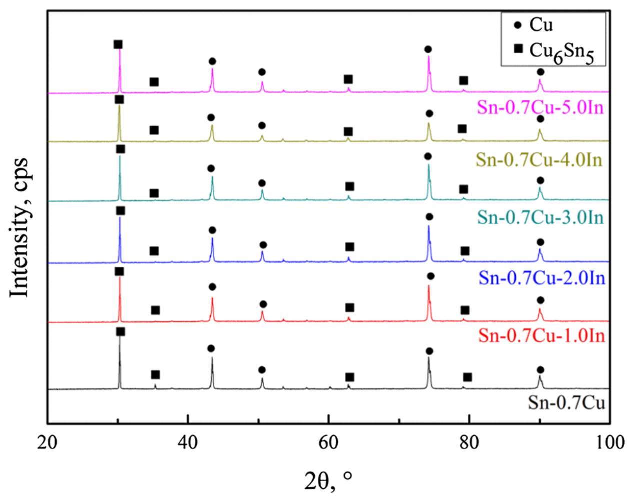

Fig. 3 XRD patterns of the IMCs on Sn–0.7Cu–xIn/Cu interface

in Fig. 2e, h have the same crystal structure as Cu_6Sn_5. The atom percentage of IMCs at solder/Cu interface was shown in Table 2. According to the atom percentage in Table 2, the ratio between Cu and (Sn,In) was about 6 to 5, indicating that $Cu_6(Sn,In)_5$ IMCs formed with indium addition. The increasing indium content in Sn–0.7Cu solder from 1.0 to 5.0 wt% leaded to an increase in the percentage of indium atoms in as-soldered $Cu_6(Sn,In)_5$ IMCs layer from 0.43 to 1.54 at%. During soldering, Sn atoms in liquid Sn–0.7Cu solder reacted with Cu atoms and formed Cu_6Sn_5 IMCs layer according to the following equation:

$$6Cu + 5Sn \rightarrow Cu_6Sn_5 \quad (1)$$

According to Refs. [27, 28], the radii of Sn atom and In atom are 145 and 155 pm. Furthermore, Sn and In share the consistent crystal structure. The similar atomic radii and consistent crystal structure usually created the atomic substitution. At the initial stage of soldering, Some Sn atoms which involved in the reaction at interface were replaced by In atoms and Cu_6Sn_5 transformed to $Cu_6(Sn,In)_5$ phase. This similar phenomenon such as the formation of interfacial $(Cu,Ni)_6Sn_5$ phase was also observed when soldering Ni-containing solder on Cu substrate [9, 11, 29].

Table 2 EDX results of IMCs at solder/Cu interface

Solder alloy	Cu, at%	Sn, at%	In, at%	Cu:(Sn,In)
Sn–0.7Cu	54.82	45.18	ND	6.06:5
Sn–0.7Cu–1.0In	54.77	44.81	0.43	6.05:5
Sn–0.7Cu–2.0In	54.31	44.77	0.92	5.94:5
Sn–0.7Cu–3.0In	54.67	44.35	0.98	6.03:5
Sn–0.7Cu–4.0In	55.18	43.52	1.30	6.15:5
Sn–0.7Cu–5.0In	54.53	43.93	1.54	5.99:5

Regarding the shape of interfacial IMCs layer shown in Fig. 2, the scallop shaped layer suggesting that the morphology of as-soldered layer was independent on the composition of the Sn–0.7Cu–xIn solder alloys. Differing from the document in Ref. [30], a uniform layer of IMCs formed between Sn–0.7Cu–0.05Ni solder and Cu substrate after soldering. The morphology of as-soldered IMC layer is still inconclusive which is needed to be further investigated. Figure 4 shows the thickness of interfacial IMCs layer after soldering between Sn–0.7Cu–xIn and Cu substrate. With the increase of indium content, the thickness of interfacial IMCs layer decreased slightly. The thickness ranged from 2.5 to 3.0 µm, suggesting that indium addition has little influence on the thickness of interfacial IMCs in the soldering stage.

3.2 IMC growth during solid aging

Figure 5 shows the interfacial microstructure of Sn–0.7Cu–xIn solder reacted with Cu substrate after aging at 150 °C for 960 h. Compared with the as-prepared interfaces shown in Fig. 2, the scallop shaped IMCs were flattened after aging. The grooves of scallop shaped grains in as-soldered interfaces provided the convenient diffusion path for Sn and Cu atoms to pass through the interfacial layer. Moreover, the transformation from scallop to planar shaped could decrease the interfacial energy, resulting in a more stable IMC layer.

It is interesting to find that indium atom percentage in $Cu_6(Sn,In)_5$ increased after aging for 960 h as shown in Table 3. The solubility of indium in $Cu_6(Sn,In)_5$ IMCs layer increased with the increasing of indium content in solder. According to the Fick's laws, the atomic flux at solder/Cu_6Sn_5 interface can be expressed by:

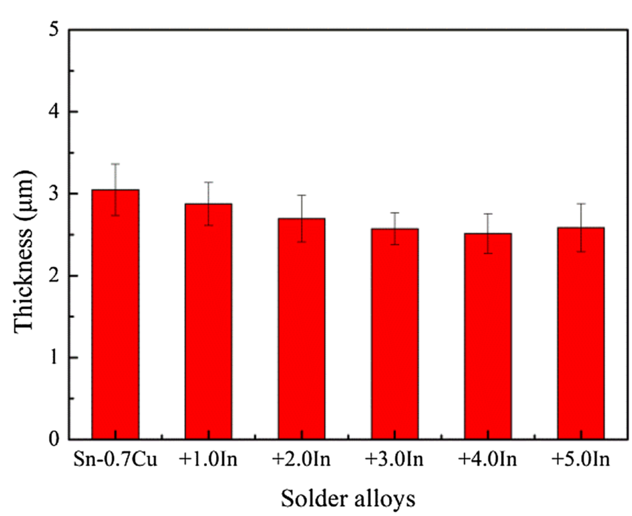

Fig. 4 Thickness of interfacial IMCs layer after soldering

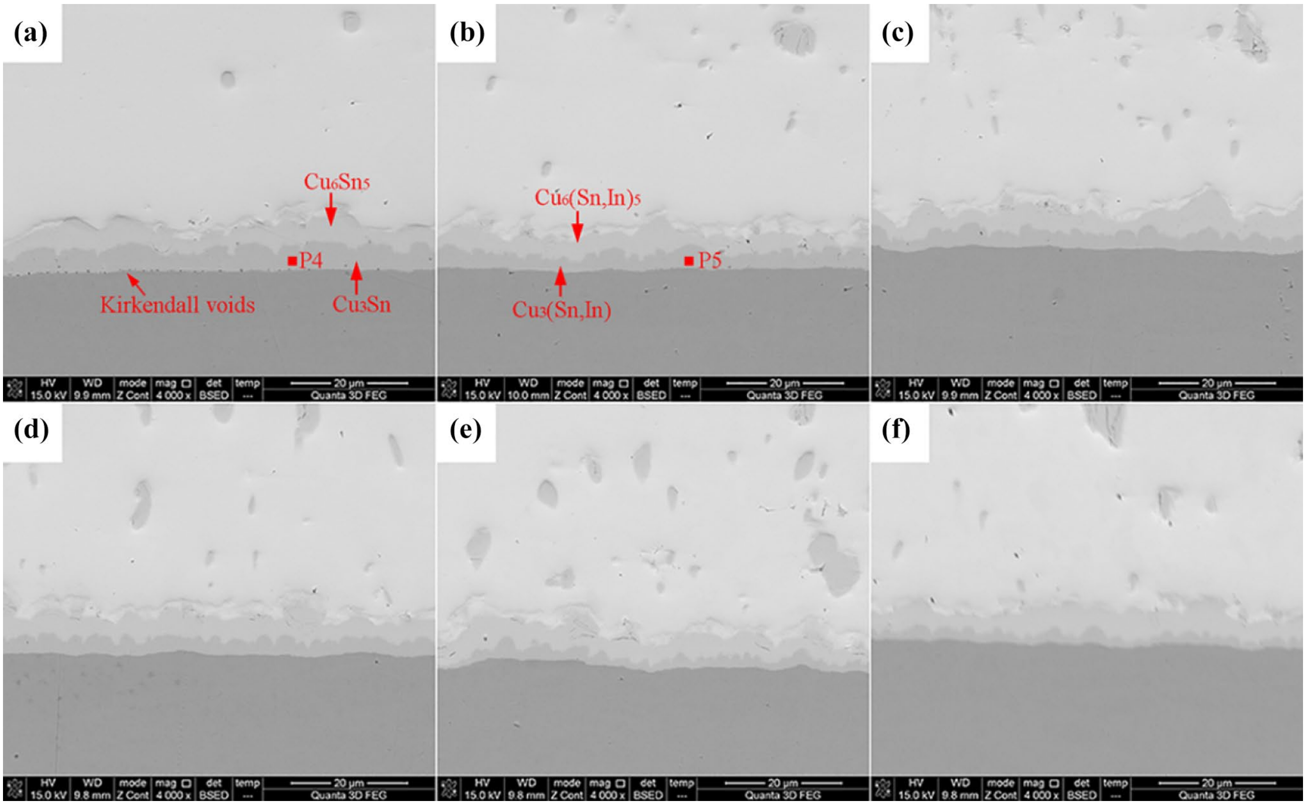

Fig. 5 Microstructure of IMCs layer after aging at 150 °C for 960 h: **a** Sn–0.7Cu; **b** Sn–0.7Cu–1.0In; **c** Sn–0.7Cu–2.0In; **d** Sn–0.7Cu–3.0In; **e** Sn–0.7Cu–4.0In and **f** Sn–0.7Cu–5.0In

Table 3 Atom percentage in interfacial $Cu_6(Sn,In)_5$ after aging for 960 h

Solder alloy	Aging temperature, °C	Cu, at%	Sn, at%	In, at%	Intermetallics
Sn–0.7Cu–1.0In	150	55.83	42.73	1.43	$Cu_6(Sn_{0.96},In_{0.04})_5$
	170	55.52	42.95	1.53	
	190	55.40	43.06	1.54	
Sn–0.7Cu–4.0In	150	56.27	38.86	4.87	$Cu_6(Sn_{0.89},In_{0.11})_5$
	170	57.13	38.07	4.80	
	190	56.96	38.31	4.72	
Sn–0.7Cu–5.0In	150	56.41	38.70	4.89	$Cu_6(Sn_{0.89},In_{0.11})_5$
	170	55.71	39.38	4.90	
	190	55.48	39.59	4.94	

$$J = -D(\partial C/\partial x) \tag{2}$$

where J is the indium atomic flux at solder/Cu_6Sn_5 interface, D is the diffusion coefficient of indium atom, $\partial C/\partial x$ is the indium atomic concentration gradient at solder/Cu_6Sn_5 interface.

With the increase of indium content, the concentration gradient of indium atomic increased at solder/Cu_6Sn_5 interface. When the concentration of indium reached balance at interface, more indium atoms would pass through the interface and substitute the Sn atoms in Cu_6Sn_5. Hence, more indium atoms were detected in $Cu_6(Sn,In)_5$ IMCs layer. The indium solubility (about 4.9 at%) found in this study reached a maximum value when indium beyond 4.0 wt%. The maximal solubility of indium in $Cu_6(Sn,In)_5$ suggesting that the average composition of $Cu_6(Sn,In)_5$ phase was $Cu_6(Sn_{0.89},In_{0.11})_5$. The maximal solubility of indium in $Cu_6(Sn,In)_5$ after aging at three different temperatures remain about the same, indicating the maximal solubility of indium in Cu_6Sn_5 is independent of aging temperature.

In Fig. 5a, a new interfacial IMCs layer formed between Cu_6Sn_5 and Cu substrate during aging. According to the EDX analysis in Fig. 6a, the new layer was confirmed as Cu_3Sn IMCs. Voids were found between Cu_3Sn layer and Cu substrate in Fig. 5a, indicating Kirkendall voids formed after long time aging. In Cu/Sn diffusion couple, the dominant diffusing component in Cu_6Sn_5 and Cu_3Sn is Sn and Cu respectively. During soldering, Sn atoms diffused through Cu_6Sn_5 and reacted with Cu substrate to form Cu_3Sn IMCs, as expressed in Eq. (3). After Cu_3Sn layer forming, Cu atoms as the dominant diffusing component diffused through Cu_3Sn layer and reacted with Cu_6Sn_5 to further increasing the thickness of Cu_3Sn layer, as expressed in Eq. (4). Due to the Cu diffusion in Cu_3Sn, Kirkendall voids formed in the interface between Cu_3Sn and Cu substrate. It has been reported that the growth of Cu_3Sn leads to the formation of a large number of Kirkendall voids [31]. Voids are undesirable defects in solder joints, therefore it is of reliability propose to restrict the growth of Cu_3Sn.

$$Sn + 3Cu \rightarrow Cu_3Sn \tag{3}$$

$$Cu_6Sn_5 + 9Cu \rightarrow 5Cu_3Sn \tag{4}$$

After indium addition as shown in Fig. 5b–f, the IMC layer between $Cu_6(Sn,In)_5$ and Cu was confirmed as $Cu_3(Sn,In)$ as shown in Fig. 6b. Table 4 summarizes the atom percentage of interfacial $Cu_3(Sn,In)$ after aging for 960 h. With the increase of indium content, the solubility of indium in $Cu_3(Sn,In)$ IMCs layer increased. In Sn–0.7Cu–5.0In/Cu couple, the maximal solubility of indium in $Cu_3(Sn,In)$ was about 3.10 at% which was slightly lower than that in $Cu_6(Sn,In)_5$ and the average composition of $Cu_3(Sn,In)$ was $Cu_3(Sn_{0.88},In_{0.12})$. Meanwhile, the maximal solubility of indium in Cu_3Sn was also independent of aging temperature.

With the increase of indium content in Sn–0.7Cu solder, the growth of Cu_3Sn IMCs layer was depressed obviously as shown in Fig. 5b–f. The thicknesses of Cu_3Sn layer after aging were measured and summarized in Fig. 7. The growth rate of Cu_3Sn was slow when the aging temperature was 150 °C as shown in Fig. 7a. It can be seen in Fig. 7b, c that the growth rate was increased rapidly with the increase of aging temperature. The thickness of Cu_3Sn at Sn–0.7Cu/Cu interface was about 10.57 μm after 960 h aging at 190 °C. Compared with the thickness about 3.46 μm at Sn–0.7Cu–5.0In/Cu interface, the growth rate of Cu_3Sn was much slower with 5.0 wt% indium addition.

The correlation between the thickness of interfacial IMCs layer and aging time can be expressed as the diffusion controlled kinetics in which *D* following Arrhenius equation:

$$X = X_0 + \sqrt{Dt} \tag{5}$$

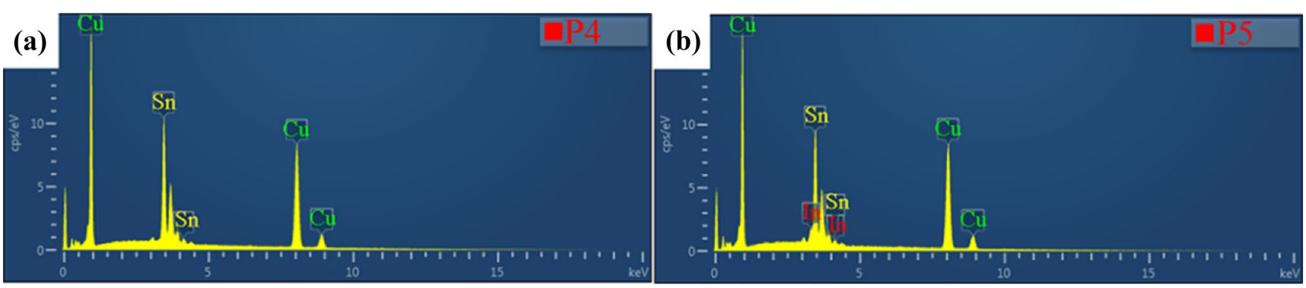

Fig. 6 Composition of IMCs layer after aging: **a** between Cu_6Sn_5/Cu; **b** between $Cu_6(Sn,In)_5$/Cu

Table 4 Atom percentage in interfacial $Cu_3(Sn,In)$ after aging for 960 h

Solder alloy	Aging temperature, °C	Cu, at%	Sn, at%	In, at%	Intermetallics
Sn–0.7Cu–1.0In	150	74.48	24.12	1.10	$Cu_3(Sn_{0.96},In_{0.04})$
	170	74.65	24.34	1.01	
	190	74.01	24.95	1.04	
Sn–0.7Cu–4.0In	150	75.36	21.93	2.71	$Cu_3(Sn_{0.89},In_{0.11})$
	170	74.84	22.39	2.77	
	190	75.69	21.64	2.67	
Sn–0.7Cu–5.0In	150	74.06	22.84	3.10	$Cu_3(Sn_{0.88},In_{0.12})$
	170	74.50	22.44	3.06	
	190	74.26	22.65	3.09	

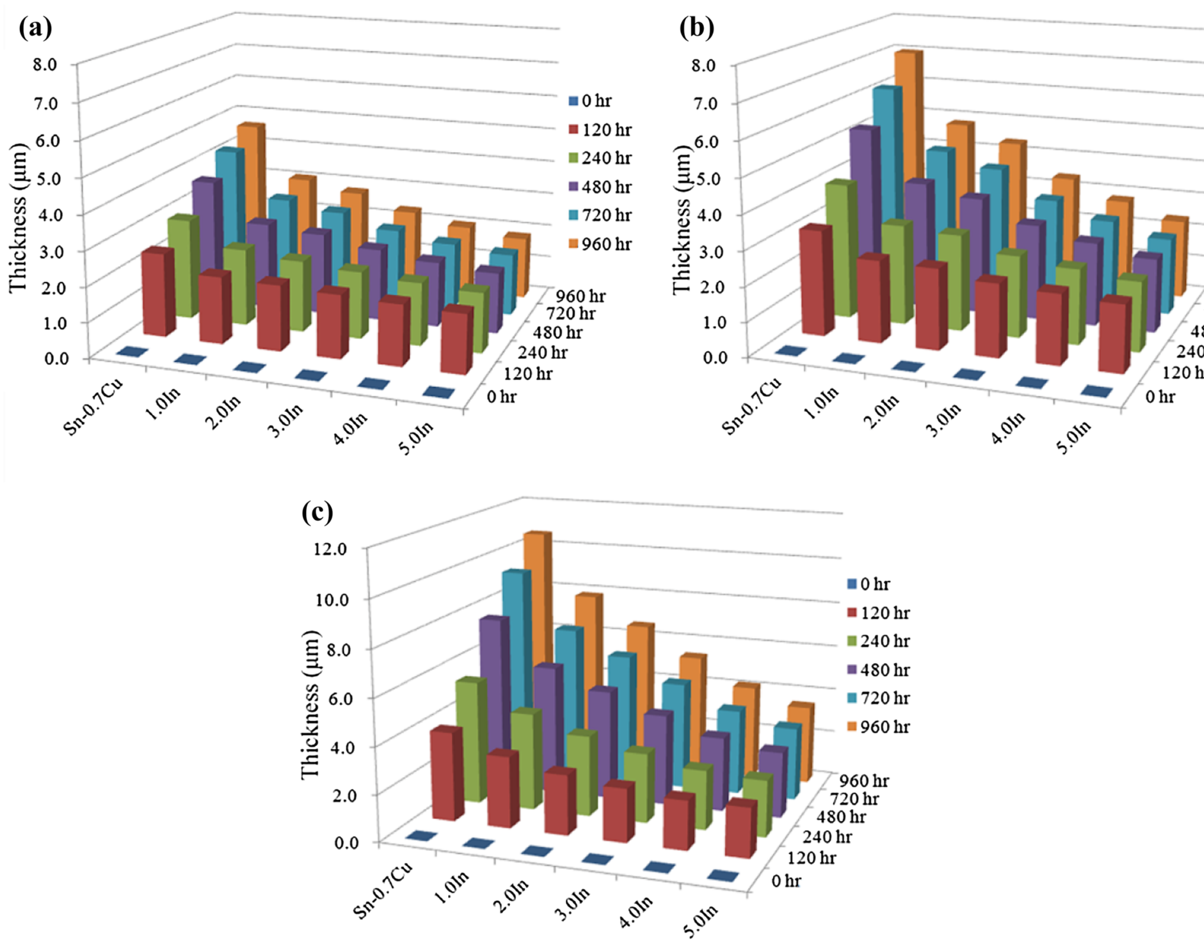

Fig. 7 Thickness of Cu_3Sn layer aged at: **a** 150 °C; **b** 170 °C and **c** 190 °C

$$D = D_0 e^{-Q/RT} \quad (6)$$

where X is the thickness of IMC layer, X_0 is the IMC layer at $t=0$ and D is the diffusion coefficient dependent on temperature variable, t is aging time, D_0 is diffusion constant, Q is activation energy, R is gas constant and T is the absolute temperature. The activation energy Q for the growth of interfacial layer can be obtained by multivariable linear regression analysis:

$$\ln D = \ln D_0 - \frac{Q}{RT} \quad (7)$$

The value of activation energy Q is obtained from the slope of Eq. (7). The diffusion coefficient D and activation energy Q for the growth of Cu_3Sn during isothermal aging were calculated with the results listed in Table 5. The diffusion coefficient of Cu_3Sn in Sn–0.7Cu/Cu couple was calculated to be 1.88E−9, 3.24E−9 and 5.54E−9 m $s^{-1/2}$ at 150, 170 and 190 °C respectively as shown in Fig. 8a. The higher the diffusion coefficient is, the faster the Cu_3Sn IMC grows. It can be seen that the growth of Cu_3Sn IMC was easier at higher temperature. With the addition of indium, the diffusion coefficient decreased compared with Sn–0.7Cu/Cu couple at the same aging temperature as shown in Fig. 8b–f.

With the increase of indium content, the diffusion coefficient in Sn–0.7Cu–xIn/Cu couples decreased. According to Eq. (7), the activation energy for the growth of Cu_3Sn was calculated to be 44.10 kJ mol^{-1}. After indium addition, the activation energy increased obviously as shown in Fig. 9. With the increase of indium content, the activation energy increased from 58.66 to 94.77 kJ mol^{-1}. Therefore, adding indium into Sn–0.7Cu was beneficial to depress the growth of Cu_3Sn IMC, and the growth rate continuously decreased with the increase of the indium content.

It has been reported that some microalloying elements would substituted the compositional atom of interfacial IMCs with lower thermodynamic affinity, forming a new IMCs with higher stability. In Refs. [25, 32], the addition of Zn element made the interfacial IMCs transform from Cu_6Sn_5 to $Cu_6(Sn,Zn)_5$ which owns lower Gibbs free energy, as well as depressed the growth of Cu_3Sn. The

Table 5 Diffusion coefficient and the activation energy of Cu_3Sn IMCs in Sn–0.7Cu–xIn/Cu couples

solder	Intermetallics	T (°C)	D (m s$^{-1/2}$)	Q (kJ mol^{-1})
Sn–0.7Cu	Cu_3Sn	150	1.88E−9	44.10
		170	3.24E−9	
		190	5.54E−9	
Sn–0.7Cu–1.0In	$Cu_3(Sn_{0.96},In_{0.04})$	150	9.12E−10	58.66
		170	2.03E−9	
		190	3.89E−9	
Sn–0.7Cu–2.0In	$Cu_3(Sn_{0.94},In_{0.06})$	150	7.22E−10	63.06
		170	1.66E−9	
		190	3.39E−9	
Sn–0.7Cu–3.0In	$Cu_3(Sn_{0.92},In_{0.08})$	150	4.19E−10	72.81
		170	1.04E−9	
		190	2.51E−9	
Sn–0.7Cu–4.0In	$Cu_3(Sn_{0.89},In_{0.11})$	150	2.16E−10	83.68
		170	6.53E−10	
		190	1.70E−9	
Sn–0.7Cu–5.0In	$Cu_3(Sn_{0.88},In_{0.12})$	150	1.09E−10	94.77
		170	3.35E−10	
		190	1.12E−9	

transformation from stable $Cu_6(Sn,In)_5$ to $Cu_3(Sn,In)$ was more difficult compared to that from Cu_6Sn_5 to Cu_3Sn. Therefore, the growth of $Cu_3(Sn,In)$ was slower than that of Cu_3Sn with indium addition.

3.3 Bending properties of Sn–0.7Cu–xIn solder joints

Figure 10 shows the influence of aging time and indium addition on the maximum bending load of Cu/Sn–0.7Cu–xIn/Cu solder joints. With the increase of aging time, bending strength decreased obviously. In as-soldered Sn–0.7Cu solder joints, bending strength was about 2.1 N. After aging at 190 °C for 240 h, the bending strength decreased to 1.6 N seriously. The bending strength stabilized at approximately 1.3 N after aging for 480 h. Indium addition plays a beneficial role in increasing the bending strength of solder joints. With the increase of indium content, joints strength showed an increasing trend, followed by a continuous decrease. The maximum bending load of In-containing joints was 2.8 N when the indium content was 3.0 wt%. When increasing the indium content to 5.0 wt%, the bending strength decreased to 2.3 N. In all cases, the joints strength of In-containing solder joints was higher than that of Sn–0.7Cu solder joints. Aging plays a detrimental effect on the bending strength of In-containing joints. The maximum bending load decreased with the increase of aging time and then stabilized after aging for 480 h. Fig. 10 also presents the fracture mode of each solder joint after aging. The empty symbol was expressed as the ductile fracture indicating the cracks were propagated in the solder matrix. The half solid symbol was represented as the partly ductile fracture indicating the cracks were propagated in the solder matrix and interfacial IMCs. The Sn–0.7Cu solder joints showed a ductile fracture in as-soldered joints and the joints aged for 240 and 480 h. After aging for 720 h, the joints showed a partly ductile fracture mode. After the addition of indium, the fracture mode did not show a partly ductile fracture until aging for 960 h. When the indium content was more than 3.0 wt%, cracks always initiated and propagated in the solder matrix. It can be concluded that indium addition apparently slowed down the fracture mode transforming from ductile fracture to partly ductile fracture. Considering both the cost and mechanical properties before and after isothermal aging, 3.0 wt% was given as the optimum indium addition amount in Sn–0.7Cu solder.

Figure 11 shows the cracks propagation during bending test and fracture morphologies of Sn–0.7Cu solder joints. In as-soldered Sn–0.7Cu joints, the cracks initiated and propagated along the interfaces between solder and Cu substrate as shown in Fig. 11a. Residual solder was observed on the top of scallop shaped Cu_6Sn_5, indicating the cracks were initiated and propagated in the solder matrix. Figure 11d, g show the fracture morphologies of Sn–0.7Cu solder joints after bending test. The fracture surfaces showed a typical ductile feature in which dimples were observed on the surface. Cu_6Sn_5 IMCs were found in the dimples as shown in Fig. 11d. In as-soldered Sn–0.7Cu solder joints, the interfacial IMCs were extremely thin and the strength of solder matrix was much higher than the bonding strength of solder matrix and IMCs. As a consequence, the bonding area between solder matrix and IMCs became weak and cracks

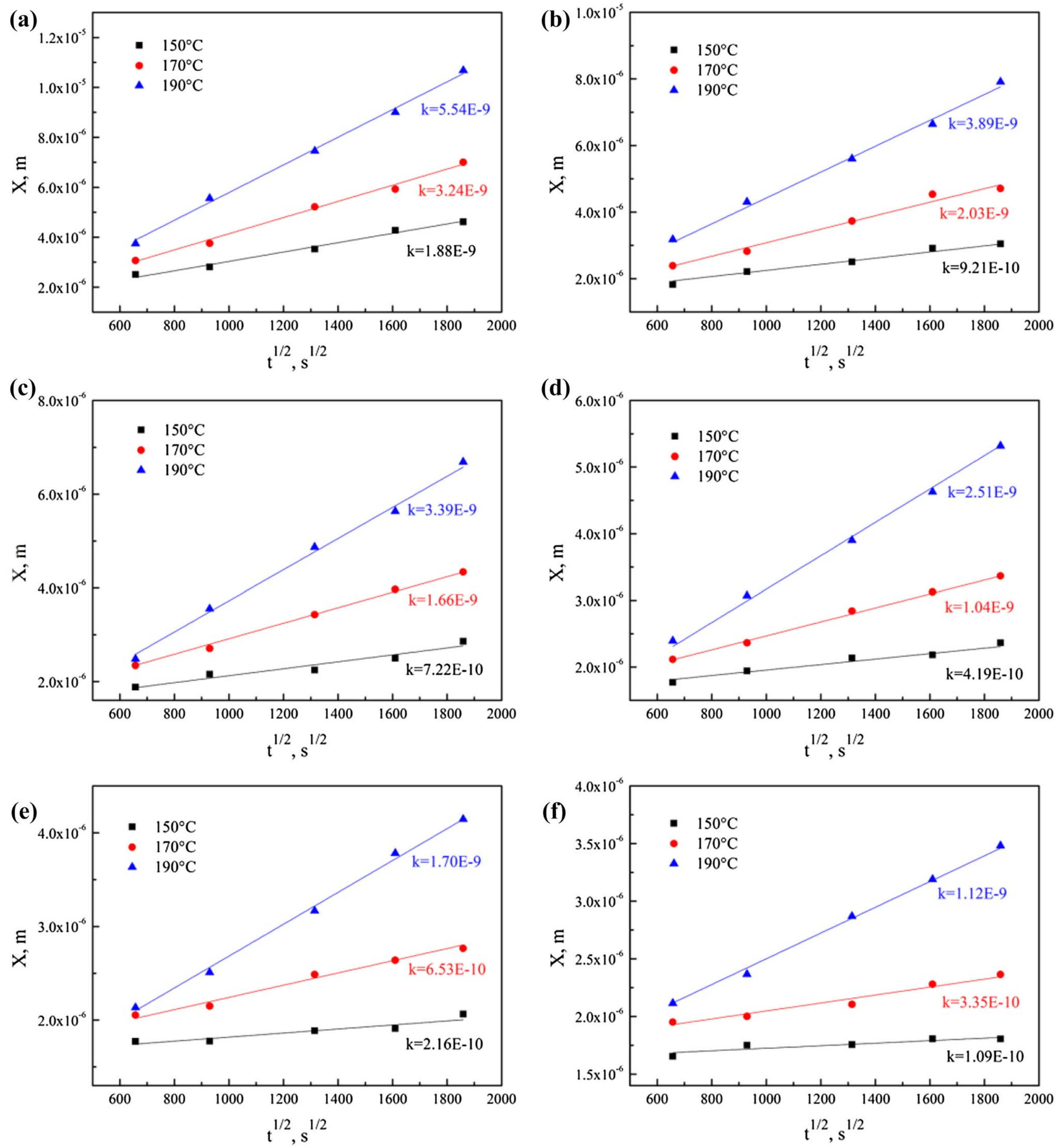

Fig. 8 Growth rate of Cu_3Sn IMCs layer: **a** Sn–0.7Cu/Cu; **b** Sn–0.7Cu–1.0In/Cu; **c** Sn–0.7Cu–2.0In/Cu; **d** Sn–0.7Cu–3.0In/Cu; **e** Sn–0.7Cu–4.0In/Cu and **f** Sn–0.7Cu–5.0In/Cu

were liable to initiate and propagate in the solder matrix near the interface. After aging for 480 h, the cracks were observed in the solder matrix as shown in Fig. 11b. Deep dimples were found on the fracture surface as presented in Fig. 11e, h. It has been documented that the dispersive distribution of fine Cu_6Sn_5 particles in as-cast Sn–0.7Cu solder would aggregate and grow into bulk Cu_6Sn_5 under thermal aging, deteriorating the mechanical properties [15, 33, 34]. The function of dispersion strengthening was weak after long time aging, reducing the mechanical properties

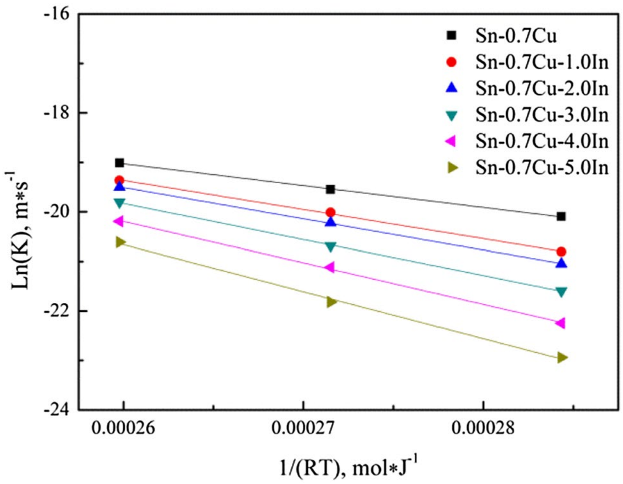

Fig. 9 Growth activation energy of Cu_3Sn IMCs layer

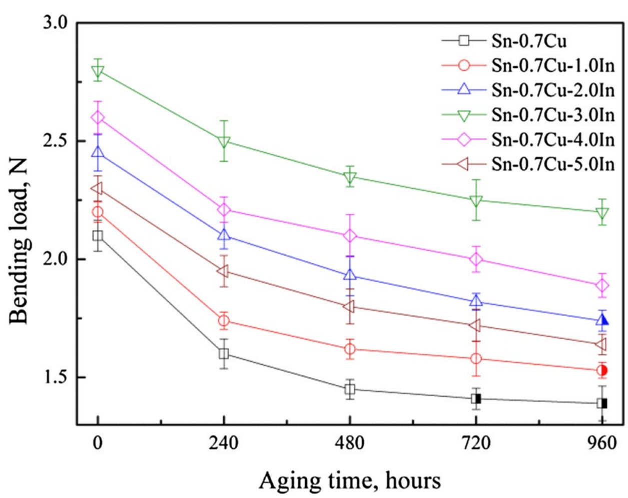

Fig. 10 The maximum bending load and fracture mode of Sn–0.7Cu–xIn solder joints

including the strength and hardness. After aging for 480 h, the strength of solder matrix was less than the bonding strength of interfaces. Therefore, cracks were initiated and propagated in the solder matrix. After aging for 960 h, the crack was initiated in the solder matrix and then propagated in the interfacial IMCs layer which can be seen in Fig. 11c. According to the fracture morphologies of Sn–0.7Cu joints aged for 960 h as presented in Fig. 11f, i, Sn–0.7Cu solder, Cu_6Sn_5 and Cu_3Sn IMCs were detected on the fracture surface. From the two sides of fracture surfaces, Cu_3Sn IMCs were exposed indicating the cracks have been propagated in the Cu_3Sn IMCs layer. The fracture of intermetallics usually exhibits typical brittle-fracture features which is a risky mode of fracture. The growth of Cu_3Sn layer resulted in the formation of Kirkendall voids which deteriorated the mechanical properties of the solder joints. It can be concluded that slowing the growth rate of Cu_3Sn IMCs layer would be helpful to improve the reliability of solder joints.

For In-containing solder joints, the cracks propagation and fracture morphologies of Sn–0.7Cu–1.0In and Sn–0.7Cu–5.0In solder joints are shown in Fig. 12 with aging for 960 h. Cracks were detected in the solder matrix and interfacial IMCs layer as shown in Fig. 12a. However, unlike the interfacial cracks in Fig. 11c, the cracks was propagated along the $Cu_6(Sn,In)_5$ IMCs layer with 1.0 wt% indium addition into the solder. Cracks were not observed in the $Cu_3(Sn,In)$ IMCs layer due to its lower growth rate compared with the Cu_3Sn IMCs. The fracture morphologies of Sn–0.7Cu–1.0In solder joints were presented in Fig. 12b, c. Besides the typical dimples characteristic, plate-like IMCs were observed on the edge of the fracture surfaces. According to the EDX profile, the plate-like IMCs were confirmed as $Cu_6(Sn,In)_5$. It can be concluded that after 1.0 wt% indium adding into the solder, cracks were initiated and propagated in the solder matrix and $Cu_6(Sn,In)_5$ IMCs layer, showing a partly ductile fracture. With the increasing indium content, evidence found in Sn–0.7Cu–5.0In solder joints suggested a ductile fracture after aging for 960 h. Crack was initiated and propagated in the solder matrix as shown in Fig. 12d. IMCs were not exposed on the fracture surface indicating a ductile fracture occurred during bending as shown in Fig. 12e, f. The rapid spread of cracks in the brittle intermetallics would accelerate the failure of solder joints during deformation. Indium addition can suppress the growth of Cu_3Sn and Kirkendall voids effectively. The initiation and propagation of cracks in IMCs layer were prevented after long time aging with the addition of indium.

4 Conclusion

The interfacial microstructure and bending properties of Cu/Sn–0.7Cu–xIn/Cu solder joints under solid aging were investigated. The diffusion coefficient and the activation energy of Cu_3Sn IMCs in Sn–0.7Cu–xIn/Cu couples were calculated. The conclusions are drawn as follows:

1. After indium addition, needle-like Cu–In–Sn IMCs were observed instead of scalloped-like Cu_6Sn_5 at the interface of as-soldered Sn–0.7Cu–xIn solder joints. The Cu–In–Sn IMCs were confirmed as $Cu_6(Sn,In)_5$ IMCs. Meanwhile, the thickness of interfacial layers in as-soldered solder joints decreased slightly with the increase of indium content.
2. During solid aging, Cu_3Sn IMCs layer formed and Kirkendall voids were observed at the interface between Cu_3Sn and Cu substrate. With the indium

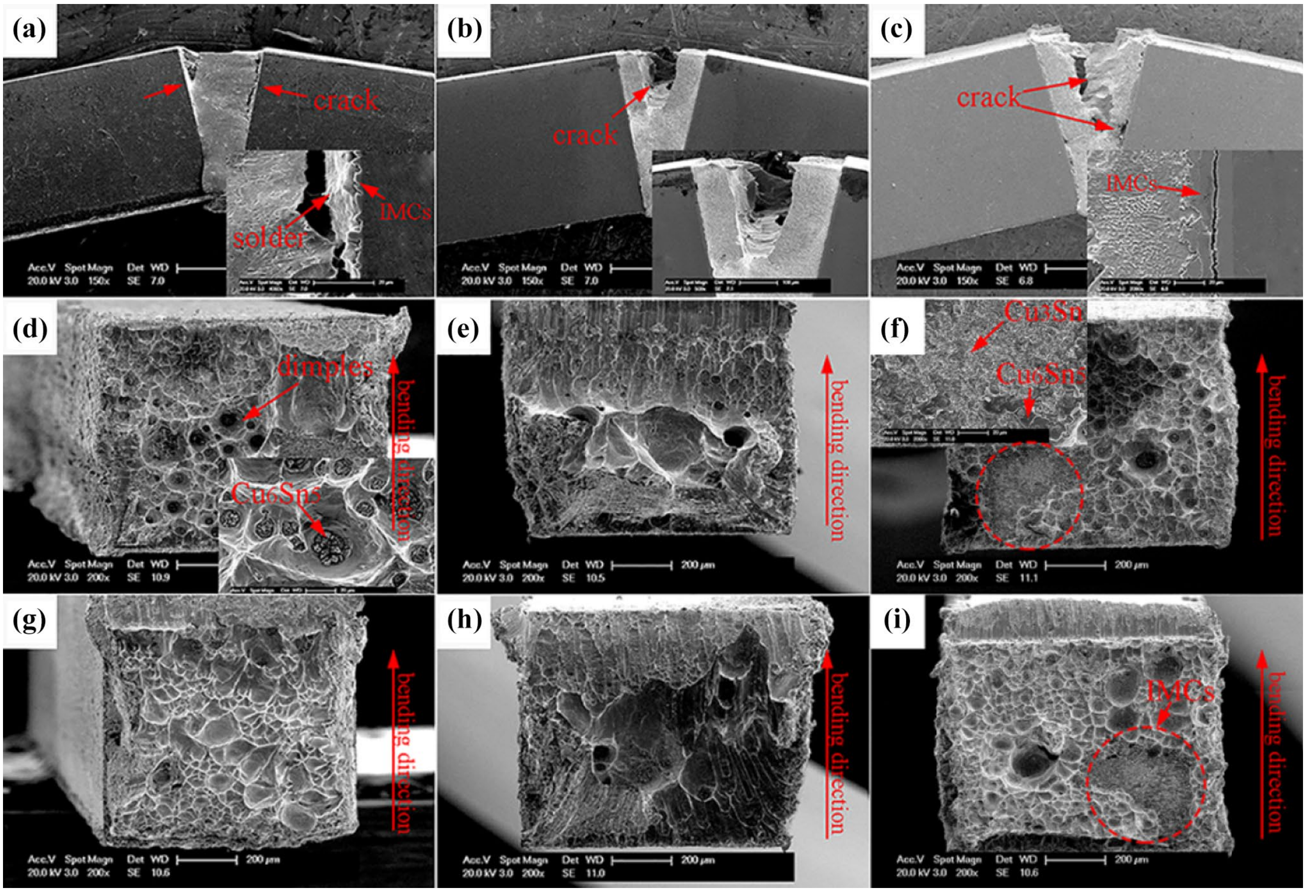

Fig. 11 Cracks propagation and fracture morphologies of Cu/Sn–0.7Cu/Cu solder joints: **a, d, g** as-soldered; **b, e, h** aged for 480 h; **c, f, i** aged for 960 h

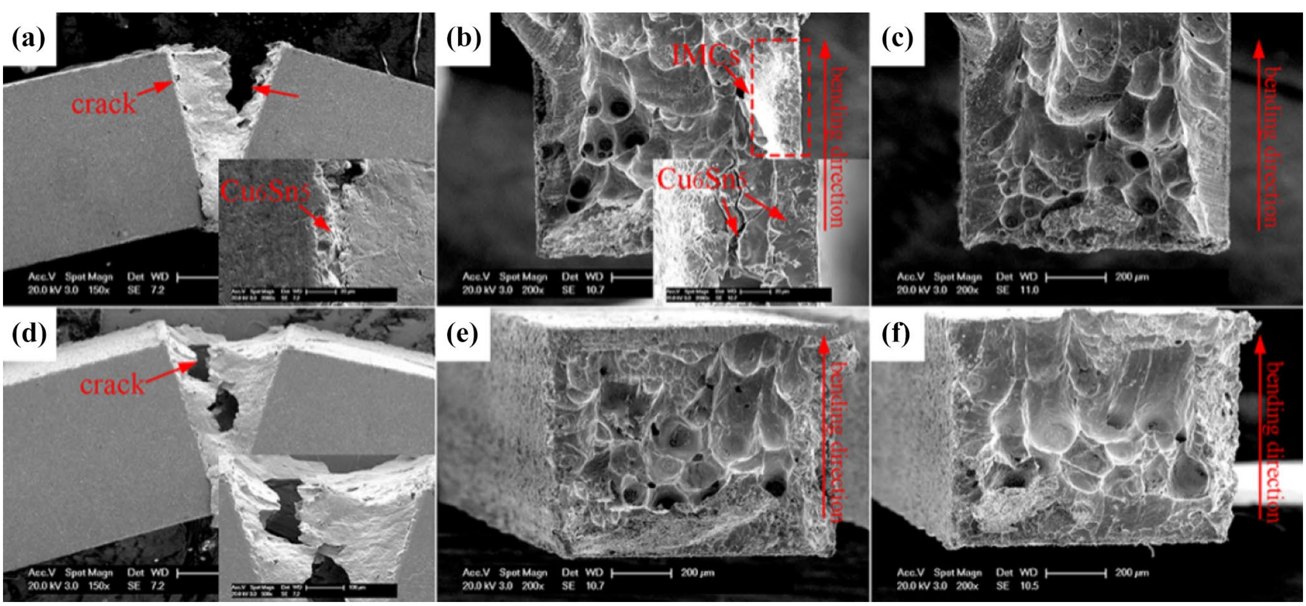

Fig. 12 Cracks propagation and fracture morphologies of Sn–0.7Cu–1.0In and Sn–0.7Cu–5.0In solder joints with aging for 960 h: **a–c** Sn–0.7Cu–1.0In; **d–f** Sn–0.7Cu–5.0In

addition, Sn atoms in Cu_3Sn IMCs were substituted by indium atoms and formed $Cu_3(Sn,In)$ IMCs. Indium addition had little influence on the growth of Cu_6Sn_5 IMCs, while strongly suppressed the growth of Cu_3Sn IMCs. In Sn–0.7Cu–5.0In/Cu couple, the maximum solubility of indium in Cu_6Sn_5 and Cu_3Sn was about 4.9 and 3.1 at.% which was independent of aging temperature. The average composition of $Cu_6(Sn,In)_5$ and $Cu_3(Sn,In)$ were given as $Cu_6(Sn_{0.89},In_{0.11})_5$ and $Cu_3(Sn_{0.88},In_{0.12})$.

3. The diffusion coefficients in Sn–0.7Cu–xIn/Cu couples were found to be lower than that of in Sn–0.7Cu/Cu couple at all experimental temperature. The activation energy for the growth of Cu_3Sn increased with the increasing indium content in Sn-0.7Cu–xIn/Cu couples.
4. Doping indium into Sn–0.7Cu solder improved the bending properties of solder joints. For Cu/Sn–0.7Cu/Cu solder joints, the maximum bending load decreased with the increase of aging time. Cracks were initiated and propagated in the solder matrix in as-soldered solder joints. After aging more than 480 h, cracks were initiated and propagated in Cu_3Sn IMCs layer and the fracture mode transformed from ductile fracture to partly ductile fracture. However, in the case of In-containing solder joints, the maximum bending load was higher than that of Sn–0.7Cu solder joints. Interfacial cracks were suppressed effectively after long time aging with indium addition.

Acknowledgements The authors would like to acknowledge the financial support by the National Natural Science Foundation of China (51004039) and the Opening Project of Jiangsu Key Laboratory of Advanced Structural Materials and Application Technology (ASMA201602).

References

1. M. Abtew, G. Selvaduray, Lead-free solders in microelectronics. Mater. Sci. Eng. R **27**, 95–141 (2000)
2. T. Laurila, V. Vuorinen, J.K. Kivilahti, Interfacial reactions between lead-free solders and common base materials. Mater. Sci. Eng. R **49**, 1–60 (2005)
3. K. Zeng, K.N. Tu, Six cases of reliability study of Pb-free solder joints in electronic packaging technology. Mater. Sci. Eng. R **38**, 55–105 (2002)
4. P. Xue, S.B. Xue, Y.F. Shen, F. Long, H. Zhu, Mechanism of reaction between Nd and Ga in Sn–Zn–0.5 Ga–xNd solder. J. Electron. Mater. **43**, 3404–3410 (2014)
5. L. Zhang, S.B. Xue, L.L. Gao, G. Zeng, Z. Sheng, Y. Chen, S.L. Yu, Effects of rare earths on properties and microstructures of lead-free solder alloys. J. Mater. Sci. **20**, 685–694 (2009)
6. L. Yang, Effects of Ag particles content on properties of Sn0.7Cu solder. J. Mater. Sci. **24**, 1405–1409 (2013)
7. Y. Li, Y.C. Chan, Effect of silver (Ag) nanoparticle size on the microstructure and mechanical properties of Sn58Bi–Ag composite solders. J. Alloys Compd. **645**, 566–576 (2015)
8. X.W. Hu, K. Li, Z.X. Min, Microstructure evolution and mechanical properties of Sn0.7Cu0.7Bi lead-free solders produced by directional solidification. J. Alloys Compd. **566**, 239–245 (2013)
9. Y.H. Lee, H.T. Lee, Shear strength and interfacial microstructure of Sn–Ag–xNi/Cu single shear lap solder joints. Mater. Sci. Eng. A **444**, 75–83 (2007)
10. A.E. Hammad, Investigation of microstructure and mechanical properties of novel Sn–0.5Ag–0.7Cu solders containing small amount of Ni. Mater. Des. **50**, 108–116 (2013)
11. H. Nishikawa, J.Y. Piao, T. Takemoto, Interfacial reaction between Sn–0.7Cu (–Ni) solder and Cu substrate. J. Electron. Mater. **35**, 1127–1132 (2006)
12. J.F. Li, P.A. Agyakwa, C.M. Johnson, Effect of trace Al on growth rates of intermetallic compound layers between Sn-based solders and Cu substrate. J. Alloys Compd. **545**, 70–79 (2012)
13. L. Zhang, J.G. Han, C.W. He, Y.H. Guo, Effect of Zn on properties and microstructure of SnAgCu alloy. J. Mater. Sci. **23**, 1950–1956 (2012)
14. T. Laurila, J. Hurtig, V. Vuorinen, J.K. Kivilahti, Effect of Ag, Fe, Au and Ni on the growth kinetics of Sn–Cu intermetallic compound layers. Microelectron. Reliab. **49**, 242–247 (2009)
15. S. Liu, S.B. Xue, Reliability study of lead-free solders under specific conditions. J. Mater. Sci. **26**, 9424–9442 (2015)
16. Z.M. Lai, D. Ye, Effect of Al on the microstructure and properties of Sn–0.7Cu solder alloy. J. Mater. Sci. **27**, 1177–1183 (2016)
17. T. Maeshima, H. Ikehata, K. Terui, Y. Sakamoto, Effect of Ni to the Cu substrate on the interfacial reaction with Sn–Cu solder. Mater. Des. **103**, 106–113 (2016)
18. Y. Wang, X. Zhao, X. Xie, Y. Gu, Y. Liu, Effects of nano-SiO_2 particles addition on the microstructure, wettability, joint shear force and the interfacial IMC growth of Sn3.0Ag0.5Cu solder. J. Mater. Sci. **26**, 9387–9395 (2015)
19. P. Xue, S.B. Xue, Y.F. Shen, H. Zhu, Interfacial microstructures and mechanical properties of Sn–9Zn–0.5 Ga–xNd on Cu substrate with aging treatment. Mater. Des. **60**, 1–6 (2014)
20. F.J. Wang, L.L. Zhou, X.J. Wang, P. He, Microstructure evolution and joint strength of Sn–58Bi/Cu joints through minor Zn alloying substrate during isothermal aging. J. Alloys Compd. **688**, 639–648 (2016)
21. C. Yu, Y. Yang, K. Wang, J. Xu, J. Chen, H. Lu, Relation between Kirkendall voids and intermetallic compound layers in the SnAg/Cu solder joints. J. Mater. Sci. **23**, 124–129 (2012)
22. Y. Tang, S.M. Luo, K.Q. Wang, G.Y. Li, Effect of Nano-TiO_2 particles on growth of interfacial Cu_6Sn_5 and Cu_3Sn layers in Sn–3.0Ag–0.5Cu–xTiO_2 solder joints. J. Alloys compd **684**, 299–309 (2016)
23. Z.M. Lai, D. Ye, Microstructure and properties of Sn–10Bi–xCu solder alloy/joint. J. Electron. Mater. **45**, 3702–3711 (2016)
24. W.K. Chio, H.M. Lee, Effect of soldering and aging time on interfacial microstructure and growth of intermetallic compounds between Sn–3.5Ag solder alloy and Cu substrate. J. Electron. Mater. **29**, 1207–1213 (2000)
25. F.J. Wang, D.Y. Li, J.H. Wang, X.J. Wang, C.H. Dong, Comparative study on the wettability and interfacial structure in Sn–xZn/Cu and Sn/Cu–xZn system. J. Mater. Sci. **28**, 1631–1643 (2017)
26. L.C. Tsao, Suppressing effect of 0.5 wt% nano-TiO_2 addition into Sn–3.5Ag–0.5Cu solder alloy on the intermetallic growth with Cu substrate during isothermal aging. J. Alloys Compd. **509**, 8441–8448 (2011)
27. J.C. Slater, Atomic radii in crystals. J. Chem. Phys. **41**, 3199–3204 (1964)

28. K. Kanlayasiri, K. Sukpimai, Effect of indium on the imtermetallic layer between low-Ag SAC0307-xIn lead-free solders and Cu substrate. J. Alloys Compd. **668**, 169–175 (2016)
29. G. Zeng, S.D. McDonald, D.K. Mu, Y. Terada, H. Yasuda, Q.F. Gu, K. Nogita, Ni segregation in the interfacial $(Cu,Ni)_6Sn_5$ intermetallic layer of Sn–0.7Cu–0.05Ni/Cu ball grid array (BGA) joints. Intermetallics **54**, 20–27 (2014)
30. H. Tsukamoto, T. Nishimura, S. Suenaga, S.D. McDonald, K.W. Sweatman, K. Nogita, The influence of solder composition on the impact strength of lead-free solder ball grid array joints. Microelectron. Reliab. **51**, 657–667 (2011)
31. C. Yu, Y. Yang, P.L. Li, J.M. Chen, H. Lu, Suppression of Cu_3Sn and Kirkendall voids at Cu/Sn–3.5Ag solder joints by adding a small amount of Ge. J. Mater. Sci. **23**, 56–60 (2012)
32. C.Y. Yu, J.G. Duh, Growth mechanisms of interfacial intermetallic compounds in Sn/Cu–Zn solder joints during aging. J. Mater. Sci. **47**, 6467–6474 (2012)
33. L. Zhang, S.B. Xue, G. Zeng, L.L. Gao, H. Ye, Interface reaction between SnAgCu/SnAgCuCe solders and Cu substrate subjected to thermal cycling and isothermal aging. J. Alloys Compd. **510**, 38–45 (2012)
34. L. Zhang, J.G. Han, C.W. He, Y.H. Gao, Reliability behavior of lead-free solder joints in electronic components. J. Mater. Sci. **24**, 172–190 (2013)